# Isotropic enhancement in the critical current density of YBCO thin films incorporating nanoscale $Y_2BaCuO_5$ inclusions

Alok K. Jha, Kaname Matsumoto, Tomoya Horide, Shrikant Saini, Paolo Mele, Ataru Ichinose, Yutaka Yoshida, and Satoshi Awaji

Citation: Journal of Applied Physics **122**, 093905 (2017); doi: 10.1063/1.5001273
View online: http://dx.doi.org/10.1063/1.5001273
View Table of Contents: http://aip.scitation.org/toc/jap/122/9
Published by the American Institute of Physics

# Isotropic enhancement in the critical current density of YBCO thin films incorporating nanoscale $Y_2BaCuO_5$ inclusions

Alok K. Jha,[1,a)] Kaname Matsumoto,[1] Tomoya Horide,[1] Shrikant Saini,[2,3] Paolo Mele,[3] Ataru Ichinose,[4] Yutaka Yoshida,[5] and Satoshi Awaji[6]
[1]*Department of Materials Science and Engineering, Kyushu Institute of Technology, Tobata-ku, Kitakyushu 804-8550, Japan*
[2]*Department of Materials Science and Engineering, University of Utah, Salt Lake City, Utah 84112, USA*
[3]*Research Center for Environmentally Friendly Materials Engineering, Muroran Institute of Technology, 050-8585 Mizumoto-cho, Muroran, Japan*
[4]*Central Research Institute of Electrical Power Industry, Yokosuka, Kanagawa 240-0196, Japan*
[5]*Department of Energy Engineering and Science, Nagoya University, Chikusa-ku, Nagoya 464-8603, Japan*
[6]*Institute for Materials Research, Tohoku University, Aoba-ku, Sendai 980-8577, Japan*

(Received 3 April 2017; accepted 22 August 2017; published online 7 September 2017)

The effect of incorporation of nanoscale $Y_2BaCuO_5$ (Y211) inclusions on the vortex pinning properties of $YBa_2Cu_3O_{7-\delta}$ (YBCO or Y123) superconducting thin films is investigated in detail on the basis of variation of critical current density ($J_C$) with applied magnetic field and also with the orientation of the applied magnetic field at two different temperatures: 77 K and 65 K. Surface modified target approach is employed to incorporate nanoscale Y211 inclusions into the superconducting YBCO matrix. The efficiency of Y211 nanoinclusions in reducing the angular anisotropy of critical current density is found to be significant. The observed angular dependence of the critical current density is discussed on the basis of mutually occupied volume by a vortex and spherical and/or planar defect. A dip in $J_C$ near the *ab*-plane is also observed which has been analyzed on the basis of variation of pinning potential corresponding to a spherical (3-D) or planar (2-D) pinning center and has been attributed to a reduced interaction volume of the vortices with a pinning center and competing nature of the potentials due to spherical and planar defects. *Published by AIP Publishing.* [http://dx.doi.org/10.1063/1.5001273]

## I. INTRODUCTION

$YBa_2Cu_3O_{7-\delta}$ (YBCO or Y123) superconducting thin films with high critical current density ($J_C$) and reduced anisotropy over varying temperature and applied magnetic field ranges are highly desired for various practical applications.[1–3] For practical applications of these superconducting films, it is important to understand the temperature and magnetic field dependence of $J_C$ and the underlying vortex pinning mechanism which determines $J_C$. The nondissipative currents under applied magnetic field can be achieved in superconducting films through pinning of flux lines. Multiple types of pinning structures are naturally evolved during growth of the films such as point defects, oxygen vacancies, stacking faults, twin planes, screw dislocations, antiphase boundaries, etc. These are termed natural pinning centers owing to their origin. The naturally grown pinning centers are weak in nature and are unable to prevent vortex motion at higher temperatures and applied magnetic fields. Feenstra *et al.*[4] have reported the role of oxygen deficiency as pinning centers and concluded that the chain-site oxygen vacancies are not strong pinning centers in high $J_C$ YBCO films. Other naturally occurring defects in YBCO films such as screw dislocations and twin-boundaries have been suggested to be the primary pinning centers although their low density does not contribute to high in-field $J_C$ of YBCO films.[5–7] It has also been reported that a high density of edge-dislocations are effective pinning centers particularly when the applied magnetic field is oriented along the *c*-axis of the YBCO film.[8]

The other kind of pinning center is the one which is intentionally incorporated into the superconducting film matrix and is thus termed artificial pinning center (APC). APCs are considered as strong pinning centers and their presence together with the naturally occurring pinning centers is desired for enhanced critical current properties over a wide range of temperature and applied magnetic field. In order to improve $J_C$ of YBCO thin films, APCs have been incorporated within the YBCO film matrix by means of different methodologies which include heavy ion irradiation,[9,10] neutron irradiation,[11,12] addition and/or substitution of rare-earth atoms,[13,14] incorporation of secondary phase nanoinclusions into the YBCO film matrix,[15–28] and decoration of the substrate surface by nanoparticles of non-superconducting materials.[29–31] These methodologies result in the formation of artificial pinning centers (APCs) within the superconducting YBCO film matrix which causes the immobilization of vortices by the APCs leading to enhanced vortex pinning properties. Among all the methods to generate APCs into the YBCO film matrix, the incorporation of non-superconducting nanoinclusions into the YBCO superconducting film matrix has been most extensively studied. The nanoinclusions of several non-superconducting materials such as $Y_2BaCuO_5$,[15,16] $Y_2O_3$,[17,18] $BaSnO_3$ (BSO),[19–21] $BaZrO_3$,[22–24] $BaIrO_3$,[25] $YBa_2TaO_6$,[26] and $YBa_2NbO_6$ (YBNO)[27,28] have been demonstrated to

[a)]E-mail: akjha@post.matsc.kyutech.ac.jp

enhance the vortex pinning properties of YBCO films deposited by the pulsed laser deposition (PLD) technique. Apart from the PLD technique, the chemical solution deposition (CSD) technique has also been successfully employed to introduce nanoinclusions of secondary phases which significantly enhance the vortex pinning properties of YBCO films.[32–36] The nanoinclusions of the secondary phases such as YBTO,[32] $BaZrO_3$ (BZO),[35] $BaHfO_3$ (BHO),[36] etc., introduced by the CSD approach are observed in the form of 3-D nanoparticles which resulted in the reduction of critical current anisotropy of YBCO films. More recently, Yamasaki *et al*. have investigated the temperature dependence of $J_C$ in YBCO films and discussed the vortex pinning properties of the nanoprecipitates and dislocations associated with stacking faults.[37–39]

The critical current density of YBCO thin films exhibits intrinsic anisotropy where at a particular magnetic field; $J_C$ along the *ab*-plane is higher than that along the *c*-axis which is attributed to the intrinsic pinning associated with the periodic modulation of the order parameter arising from the layered structure of YBCO.[40–42] The nanoinclusions of perovskite materials such as $BaZrO_3$ (BZO), $BaSnO_3$ (BSO), $YBa_2NbO_6$ (YBNO), etc., self-assemble in the form of columnar nanostructures along the *c*-axis of the films which are very effective in improving $J_C$ particularly when the magnetic field is oriented along the *c*-axis of the films. For many practical applications, the anisotropic character of $J_C$ still needs to be improved over a wide range of temperatures and applied magnetic fields.[43] It is, therefore, highly desirable to enhance the critical current density of YBCO thin films in the intermediate angular regime (between the *ab*-plane and *c*-axis) as well. For this reason, 3-dimensional artificial pinning centers (nanoparticles) are preferred over 1-dimensional artificial pinning centers (nanocolumns).

The earliest reports on the use of 3-D APCs were made by Haugan *et al*.[15] and Varanasi *et al*.[16] in which multilayers of $Y_2BaCuO_5$ (Y211) and Y123 were made and Y211 nanoparticles were found to improve the in-field critical current properties. However, the angular variation of critical current density was not studied in their report. Mele *et al*.[17] have attempted to incorporate $Y_2O_3$ nanoparticles but the anisotropy in $J_C$ could not be improved significantly. $Y_2O_3$ has been tried as 3-D APCs by other researchers also and the angular dependent $J_C$ was improved at 77 K.[44]

In this paper, detailed investigation on the effect of incorporating Y211 nanoscale inclusions on the vortex pinning properties of YBCO thin films is presented. For incorporating Y211 nanoparticles into the YBCO superconducting film matrix, the surface modified target method is employed whose details can be found elsewhere.[45] The concentration of secondary phase Y211 nanoinclusions is controlled by varying the area of the Y211 rectangular piece. The nanocomposite thin films comprising Y211 3-D APCs showed enhanced $J_C$-$H$ characteristics along with significantly improved angular dependence which is more prominent at lower temperature. In addition, the irreversibility field is calculated for all the samples and its variation with temperature is studied. The role of spherical defects in shifting the irreversibility line (IL) towards a higher $H$-$T$ regime is also discussed.

## II. EXPERIMENTAL DETAILS

A pristine YBCO film and YBCO films consisting of Y211 nanoparticles have been deposited on single crystal $SrTiO_3$ (STO) substrates using the PLD technique (KrF excimer laser, $\lambda = 248$ nm). The substrate temperature of 830 °C, repetition rate of 10 Hz, and $O_2$ partial pressure of 0.26 mbar were used for the deposition of the films. A commercial YBCO target was used to deposit the pristine YBCO film and for making YBCO + Y211 nanocomposite films, the same YBCO target is modified by putting a thin rectangular piece of Y211 onto the YBCO target by means of silver paste. An Y211 pellet was synthesized in the laboratory by the solid state reaction method and cut into thin rectangular pieces to be used in surface modified targets. Phase purity of the Y211 pellet prepared in the laboratory was ascertained by X-ray diffraction (XRD) measurement. The concentration of Y211 nanoparticles in the nanocomposite thin films is varied by modifying the target surface with three different sizes of rectangular pieces: 1.8 area%, 3.6 area%, and 5.4 area% which are referred to as Y211A, Y211B, and Y211C in this paper onwards. As the target is rotated, the Y211 portion is periodically ablated allowing the formation of Y211 nanoparticles in the YBCO film matrix.

XRD of pristine YBCO and YBCO + Y211 nanocomposite films was carried out using an X-ray diffractometer (Bruker D8 XRD) with Cu-K$\alpha$ radiation. The $\theta$–$2\theta$ diffraction data were collected over diffraction angles ranging from $2\theta = 5°$–$80°$. Slow scan XRD is again conducted over diffraction angles ranging from $2\theta = 26°$–$52°$ to look for the presence of Y211 nanoparticles in the nanocomposite thin films. $\omega$-scan and $\phi$-scan were also carried out to observe the in-plane and out-of plane symmetries. The cross-sectional and planar microstructures of the thin film samples have been observed using a transmission electron microscope (JEOL JEM-2100F).

UV photolithography and wet-chemical etching technique were employed for making microbridges on thin film samples for critical current measurements. The electrical transport properties of these thin film samples have been measured using the standard four-probe method by a Physical Property Measurement System (PPMS, Quantum Design). The distance between the current source contact points (outer probes) was 8 mm, whereas the voltage points (inner probes) were 2 mm apart. Resistivity versus temperature measurements were carried out at different applied magnetic fields to determine the critical temperature ($T_C$) and the irreversibility lines (*ILs*) for all the samples. A voltage criterion of 1 $\mu$ V cm$^{-1}$ has been used to obtain the critical current values. Angular dependence of $J_C$ of all the thin film samples was measured at different temperatures and applied magnetic fields using the same voltage criterion.

## III. RESULTS AND DISCUSSION

Pristine YBCO and YBCO + Y211 nanocomposite films have been observed to be strongly oriented along the *c*-axis direction as determined from the X-ray diffraction measurement. In order to determine the in-plane order, XRD $\phi$-scan measurements were performed. All the thin film samples

exhibit good in-plane ordering. As the sample is rotated around its *c*-axis normal, peaks separated by 90° appear. This is characteristic of the typical a/b twinning of the orthorhombic YBCO. No extra peaks, indicating the presence of misaligned grains, are visible. The *c*-axis for the YBCO films with APCs, however, exhibited relative compression compared to the pristine YBCO film. The $\Delta\omega$ of the YBCO(005) peak for all the samples varies between 0.16° and 0.24°, while $\Delta\phi$ of YBCO(102) for all samples varies between 0.64° and 0.89° exhibiting good in-plane orientation. The structural parameters as obtained from X-ray diffraction measurement for all the thin film samples are listed in Table I. In the usual $\theta$-$2\theta$ scan, the presence of Y211 nanoparticles could not be confirmed and for this reason, slow scan XRD was performed. Figure 1 shows the XRD pattern of all the thin film samples conducted over diffraction angles ranging between $2\theta = 26°$–$52°$. A small peak corresponding to Y211 (002) was observed at $2\theta = 31.6°$ in YBCO + Y211C samples which indicates that Y211 nanoparticles are epitaxially grown within the Y123 matrix. From the TEM image, it is evident that the Y211 phase is grown in the island growth mode within the epitaxial Y123 matrix. The growth orientation of the Y211 phase with respect to the Y123 phase leads us to examine the lattice mismatch between the two phases. The mismatch between $Y211_a/Y123_{ab\text{-}avg.} = -7.5\%$ whereas the mismatch between $Y211_b/Y123_{ab\text{-}avg.} = 5.45\%$. Such large lattice mismatch between the Y211 and Y123 phases is favorable for the growth of Y211 nanoparticles within the Y123 epitaxial matrix as deposition on the island nucleated phase is energetically favorable than on the lattice mismatched phase. On the other hand, the mismatch between $Y211_c/Y123_{ab\text{-}avg.} = -2.1\%$ which may lead to other growth orientation but it is not observed here. Apart from Y211 (002), another small peak corresponding to $Y_2O_3$ (400) was also observed at $2\theta = 33.8°$ in some of the samples indicating the oriented growth of the $Y_2O_3$ nanoparticles too. The formation of yttria in the thin film is observed when the precursor is rich in Yttrium. The kinetics of the deposition process may also contribute to the formation of small $Y_2O_3$ particles. Since yttria has a good in-plane match with the YBCO phase it can readily nucleate at the surface of the growing YBCO film. The orientation relationships between YBCO and $Y_2O_3$ phases are as follows: [100]YBCO || [110]$Y_2O_3$, [010]YBCO || [110]$Y_2O_3$, and [001]YBCO || [001]$Y_2O_3$. In the *ab*-plane, the lattice mismatch is less than 3% since *d*(400) $Y_2O_3$ is equal to 2.65 Å and *d*(110)YBCO is equal to 2.73 Å. The highly oriented growth of $Y_2O_3$ may be attributed to the lower interfacial energies between YBCO and $Y_2O_3$.[46] The formation of the $Y_2O_3$ phase in YBCO films deposited by the laser ablation process has been observed previously also by other researchers.[47]

TABLE I. Structural parameters for the superconducting samples as obtained from the XRD measurement.

| Composition | *c*-axis (Å) | $\Delta\omega$ (005) (deg.) | $\Delta\phi$ (102) (deg.) |
|---|---|---|---|
| YBCO | 11.697 | 0.24 | 0.89 |
| YBCO + Y211A | 11.685 | 0.21 | 0.64 |
| YBCO + Y211B | 11.687 | 0.19 | 0.75 |
| YBCO + Y211C | 11.685 | 0.16 | 0.83 |

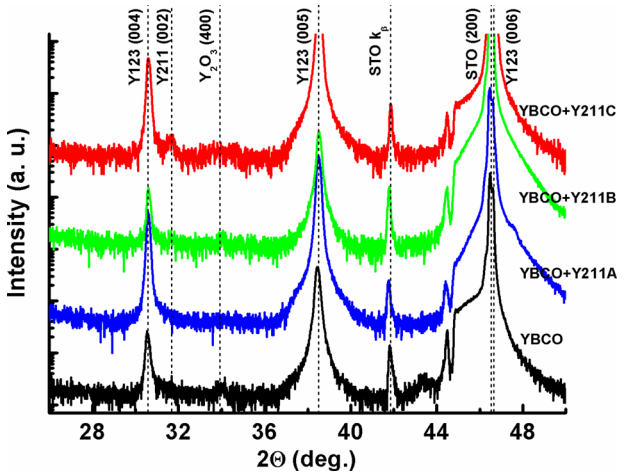


FIG. 1. XRD pattern of YBCO and YBCO + Y211 nanocomposite films recorded between $2\theta = 26°$ and 52°. A small peak at $2\theta = 31.6°$ in the XRD pattern of the YBCO + Y211C film corresponds to the (002) plane of Y211. Another small peak which appears at $2\theta = 33.8°$ in some of the samples has been attributed to the (400) plane of $Y_2O_3$.

Figure 2 shows the cross-sectional transmission electron micrographs of YBCO + Y211A (a) and (b), YBCO + Y211B (c) and (d), and YBCO + Y211C (e) and (f) nanocomposite films at two different magnifications. In all the TEM images, formation of nanoparticles can easily be observed which are supposed to be of Y211. The Y211 nanoparticles are found to be randomly dispersed in the YBCO film matrix. The density of the Y211 nanoparticles, however, seems to vary systematically with the amount of Y211 incorporated into the YBCO films. Apart from the randomly distributed nanoparticles, some planar defects are also observed which are supposed to be stacking faults originated during the growth of the film. The inclusion of nanoscale secondary phases into the Y123 matrix is expected to induce local defects which could be instrumental in the analysis of the isotropic pinning. However, the generation of such local defects due to secondary phase nanoinclusions also depends on the fabrication and crystallization process and growth mechanism. In the CSD technique, the crystallization of the phases takes place simultaneously during pyrolysis of the deposited layer. The nucleation of the secondary phase starts in the precursor itself and becomes independent of the orientation of *RE*123 layer[48] which leads to the formation of randomly oriented nanoparticles and incoherent interfaces between the phases and the density of associated defects becomes significantly high. However, in the PLD technique, the growth mode of the layers and the crystallization process are different in which surface diffusion of adatoms is high enough for the secondary phase nanoinclusions to nucleate and grow on the epitaxial Y123 matrix and the nanoscale inclusions of perovskite materials lead to the generation of semi-coherent interfaces.[35] The different growth mechanisms and the crystallization processes lead to different microstructures of YBCO nanocomposite films prepared by CSD and PLD techniques. The geometry of the secondary phase inclusions, the density of planar defects (which is very

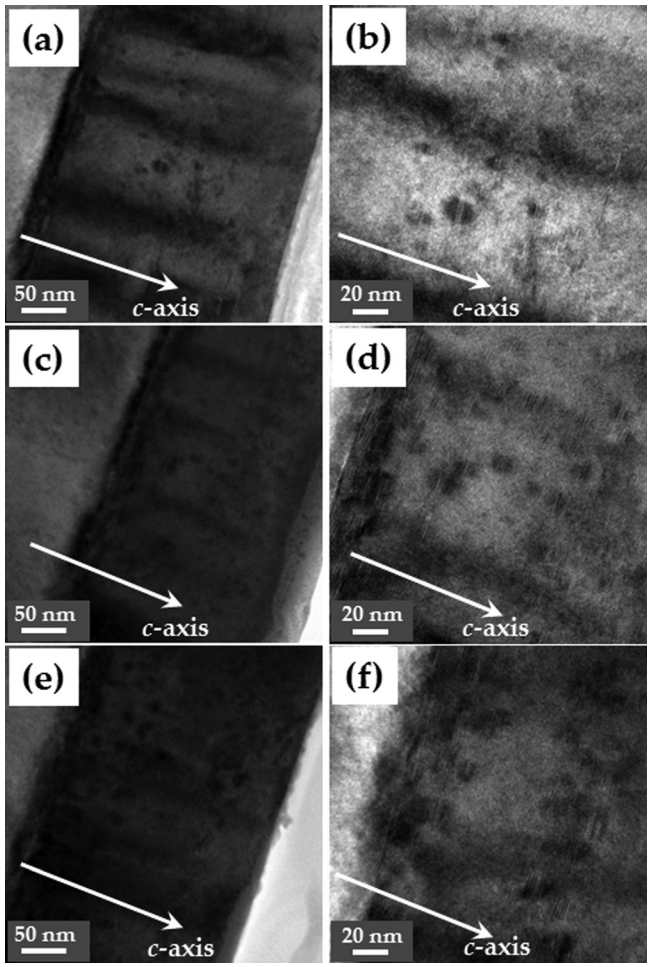


FIG. 2. The cross-sectional view of the microstructure of YBCO + Y211A (a), (b), YBCO + Y211B (c), (d) and YBCO + Y211C (e), (f) at different magnifications. The formation of spherical nanostructures together with some planar defects can be clearly observed in these images.

high in CSD films), etc., are some of the microstructural differences that can be clearly observed in films prepared by CSD and PLD techniques. Figure 3 shows the planar view of the TEM images of the YBCO + Y211B film at two different magnifications. From the planar view, uniform distribution of Y211 nanoparticles together with the presence of some twin boundaries can be observed. From the planar view of the TEM image, a rough estimation of the Y211 nanoparticle density is made which comes out to be $\sim 1.15 \times 10^{12}\,\mathrm{cm}^{-2}$. The size of the Y211 nanoscale inclusions varies between 4 and 10 nm. In Fig. 3(b), the distorted lattice planes of the YBCO film matrix around the Y211 nanoparticles can be observed which are also promising pinning centers. In Fig. 4, the cross-sectional HRTEM image of (a) YBCO + Y211B and (b) YBCO + Y211C films is shown where the presence of planar defects can be seen with lengths ranging between 50 and 100 nm. The formation of stacking faults in the YBCO film takes place naturally where an extra non-superconducting Cu-O plane evolves between adjacent YBCO unit cells normal to the *c*-axis. These stacking faults originate from the decomposition of Cu-containing impurity phases such as (Ba-Cu-O) during post-annealing of the films in an oxygen atmosphere. In the present case, since the oxygenation of all the samples was executed under the same conditions of temperature, duration, and mass flow rate, the density of the stacking faults is expected to be the same in the samples. Figure 4, in which stacking faults are marked by small white arrows, reveals that the density of stacking faults in these two films is not much different. The dimensions of the planar defects related to stacking faults have been previously shown by Llordes *et al.*[49] which is similar to the present study. However, they employed the chemical solution deposition (CSD) technique for the deposition of the films which is very different from PLD and the density of the planar defects, therefore, is very different in their case.

The $T_C$s of all the superconducting films are obtained from electrical transport measurement and are listed in Table II. The $T_C$ for the pristine YBCO film is 89.8 K, whereas for YBCO + Y211A, YBCO + Y211B, and YBCO + Y211C films, it is 89.1 K, 89.6 K, and 88.8 K, respectively. Substantial reduction in $T_C$ of the nanocomposite films is not observed in comparison to that of pristine YBCO film indicating minimum deterioration of the superconducting matrix which is also evident from the XRD measurement. It is to be noted that the YBCO + Y211B film has higher $T_C$ than that for YBCO + Y211A in contrast to the general trend among the samples. The reduction in $T_C$ may be attributed to possible interfacial strain that might have been generated during the growth of the film and this is also studied by Zhai and Chu.[50] However, as the strain is relieved by dislocations or other growth defects, this reduction is suppressed. The

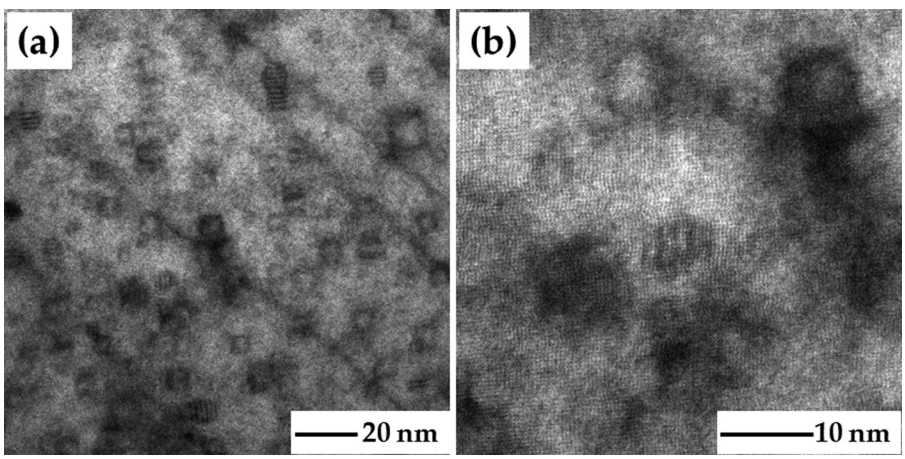


FIG. 3. The planar view of the microstructure of the YBCO + Y211B film at different magnifications. The uniform distribution of the nanoparticles and buckled lattice-planes near the interfaces can be clearly observed. Twin boundaries can also be seen which are common in YBCO films.

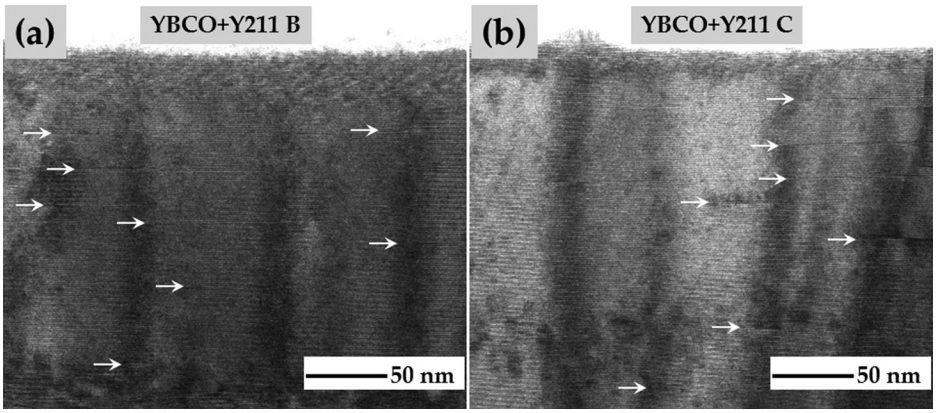


FIG. 4. Cross-section TEM image of (a) YBCO + Y211B and (b) YBCO + Y211C films exhibiting planar defects of length ranging between 50 and 100 nm indicated by small white arrows.

reduced $T_C$ of YBCO + Y211A in comparison to that for pristine YBCO film and higher $T_C$ of YBCO + Y211B in comparison to that for YBCO + Y211A film may be attributed to this phenomenon. It is, however, difficult to quantify strain in the samples and this could well be the subject of a separate study. Further, increasing APC concentration in the samples (e.g., YBCO + Y211C in the present case) may lead to reduction in the superconducting volume fraction which in turn results in reduced $T_C$. The $T_C$ reduction, therefore, is not simply related to the Y211 content but seems to be related to the strain in the samples as well.

The practical utility of superconductors depends on another important superconducting parameter called irreversibility field ($H_{irr}$) which determines the upper boundary of the critical current density. The vortex matter undergoes a solid-liquid transition across the melting line or irreversibility line (*IL*) and shifting of this line towards a higher *H-T* regime is strongly desired.[1–3,51] Figure 5 shows the variation of $\mu_0 H_{irr}$ with (a) absolute temperature $T$ and (b) reduced temperature ($T/T_C$) for all the nanocomposite films in comparison to that of the pristine YBCO film. $\mu_0 H_{irr}$ for pristine YBCO at 77 K has been estimated to be 7.8 T. In the case of the nanocomposite films, the value of $\mu_0 H_{irr}$ at 77 K is 7.8 T, 9.7 T, and 8.8 T for YBCO + Y211A, YBCO + Y211B, and YBCO + Y211C films, respectively. There is a pronounced up-shift of the *ILs* in the nanocomposite films and it becomes more prominent when $\mu_0 H_{irr}$ is plotted against reduced temperature ($T/T_C$) which eliminates the effect of transition temperature. The upward shift in the *ILs* has been discussed earlier and has been attributed to the morphology of the APCs and not simply to the volume fraction of the secondary phase inclusions acting as APCs.[45] It has been reported earlier that the straight nanocolumnar disorders are very effective in shifting of the *IL*s towards the higher *H-T* regime when the applied magnetic field is along the *c*-axis direction as the vortices can be completely occupied by nanocolumns.[52–54] Spherical nanoparticles, on the other hand, can arrest the segments of the vortices connected by kinks. The effect of nanoparticles on shifting of the *IL*s has been discussed by Miura *et al.*[55,56] where synergetic combination of twin-boundaries and BZO nanoparticles has been successfully demonstrated to shift the *IL*s towards the higher *H-T* regime. According to their analysis, the density of twin boundaries has been suggested to be directly linked to the density of BZO nanoparticles which in turn results in varying the matching field of the twin boundaries. The introduction of nanoparticles of secondary phases into the YBCO film has also been reported to influence the vertical coherence of the twin boundary resulting in reduced spacing of the twin boundaries.[57,58] We actually looked into the planar view of the microstructures of YBCO + Y211A and YBCO + Y211C films for twin-boundary density comparison. Figure 6 shows the planar view of the microstructures of YBCO + Y211A and YBCO + Y211C films which reveals that despite the density of the Y211 nanoinclusions being much different in these two films, there is no apparent difference in the density of the twin boundaries. Moreover, the density of stacking faults is also compared between YBCO + Y211B and YBCO + Y211C films in Fig. 4 and it can be observed that the density of stacking faults in these two films is significantly lower than that in the films prepared by the CSD technique. The difference in the microstructures of these films and the ones reported in the references cited above may be attributed to the different growth mechanisms in PLD and CSD films.

In our samples, a high density of twin-boundaries together with Y211 nanoparticles is present in the Y123 matrix. Although the effect of twin-boundaries on vortex pinning properties is limited to lower applied magnetic field, they can contribute in localizing the vortices together with

TABLE II. Comparison of several superconducting parameters of pristine YBCO and YBCO + Y211 nanocomposite thin films.

| Composition | $T_C$ (K) | $(J_C)$ (MA cm$^{-2}$) (77 K, 0 T) | $F_{pmax.}$ (GN m$^{-3}$) (77 K) | $B_{max.}$ (T) (77 K) | $(J_C)$ (MA cm$^{-2}$) (65 K, 0 T) | $F_{pmax.}$ (GN m$^{-3}$) (65 K) | $B_{max.}$ (T) (65 K) | $B_{irr.}$ (T) (77 K) |
|---|---|---|---|---|---|---|---|---|
| YBCO | 89.8 | 1.64 | 2.86 | 2 | 3.58 | 13.6 | 3.5 | 7.8 |
| YBCO + Y211A | 89.1 | 1.85 | 4.00 | 2 | 3.99 | 21.2 | 3.8 | 7.8 |
| YBCO + Y211B | 89.6 | 2.30 | 3.95 | 2 | 4.38 | 31.6 | 4.2 | 9.7 |
| YBCO + Y211C | 88.8 | 1.83 | 4.78 | 2.6 | 3.44 | 39.5 | 5.0 | 8.8 |

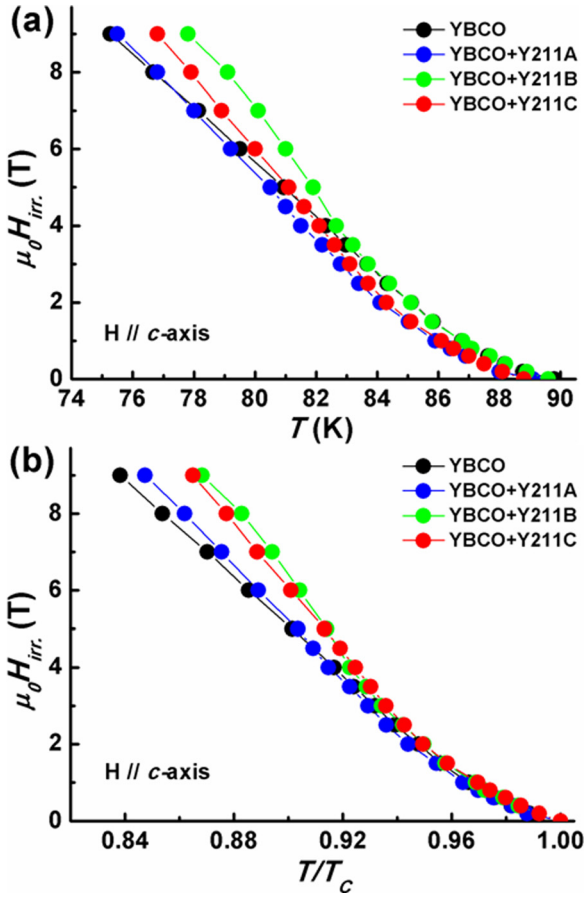


FIG. 5. Variation of irreversibility field with absolute temperature (a) and reduced temperature (b) for YBCO and YBCO + Y211 nanocomposite films.

the Y211 nanoparticles at higher applied magnetic field. At higher applied magnetic field, when vortex density is more than APC density, the enhancement in $H_{irr}$ is expected to cease. It should be noted, however, that the vortices are elastic in nature and they also interact with themselves and are arranged in a particular pattern depending on the pinning landscape present in the superconducting matrix.

Pinning force density ($F_p$) which is the product of applied magnetic field and the corresponding critical current density ($J_C$) is an important parameter which reflects the $J_C$ performance of superconducting samples under applied magnetic field. $F_{pmax}$ is the maximum $F_p$ observed for the investigated applied magnetic field range and $\mu_0 H_{max}$ is the applied field where $F_{pmax}$ emerges. Figure 7 shows the variation of $J_C$ and $F_p$ with respect to applied magnetic field for pristine YBCO and YBCO + Y211 nanocomposite films obtained at 77 K and 65 K. It can be observed that the $J_C$ -$H$ characteristics of YBCO + Y211 nanocomposite films have been improved significantly which is reflected in the higher $F_{pmax}$ values for the nanocomposite films both at 77 K and 65 K. It is also to be noted that the improvement in the $J_C$–$H$ characteristics is very systematic with respect to the density of Y211 nanoscale inclusions in the YBCO superconducting matrix which is prominently observed at 65 K. In addition to higher $F_{pmax}$ values, YBCO + Y211 nanocomposite films also exhibit $\mu_0 H_{max}$ values shifted towards higher applied magnetic fields. Although the enhancement in $F_{pmax}$ and $\mu_0 H_{max}$ values is not very high at 77 K, it is significant at 65 K. The $F_{pmax}$ value for the pristine YBCO film at 65 K is 13.6 G N m$^{-3}$, whereas it is 21.2, 31.6, and 39.5 G N m$^{-3}$ for YBCO + Y211A, YBCO + Y211B, and YBCO + Y211C nanocomposite films, respectively. $\mu_0 H_{max}$ values as obtained at 65 K for YBCO, YBCO + Y211A, YBCO + Y211B, and YBCO + Y211C films are 3.5, 3.8, 4.2, and 5.0 T, respectively. Systematic enhancement in $F_{pmax}$ and $\mu_0 H_{max}$ values of the nanocomposite films can be understood in terms of the densities of the artificial pinning centers preventing the motion of the vortices. A pinned vortex line has a lower energy than a free vortex in the superconductor. The energy gain per unit length of a vortex line, in the case of a non-superconducting particle, corresponds to the condensation energy in the core region. The total pinning energy for a vortex line, therefore, is

$$U = \frac{B_c^2}{2\mu_0}\pi\xi_{ab}^2\varepsilon(\theta)d, \tag{1}$$

where $B_c(T) = \frac{\phi_0}{2\sqrt{2}\pi\xi_{ab}(T)\lambda_{ab}(T)}$ is the thermodynamic critical field, $\phi_0$ is the flux quantum, $\xi_{ab}$ is the coherence length in the $ab$-plane, $\lambda_{ab}$ is the penetration depth along the $ab$-plane, and $d$ is the size of the non-superconducting particle. Energy

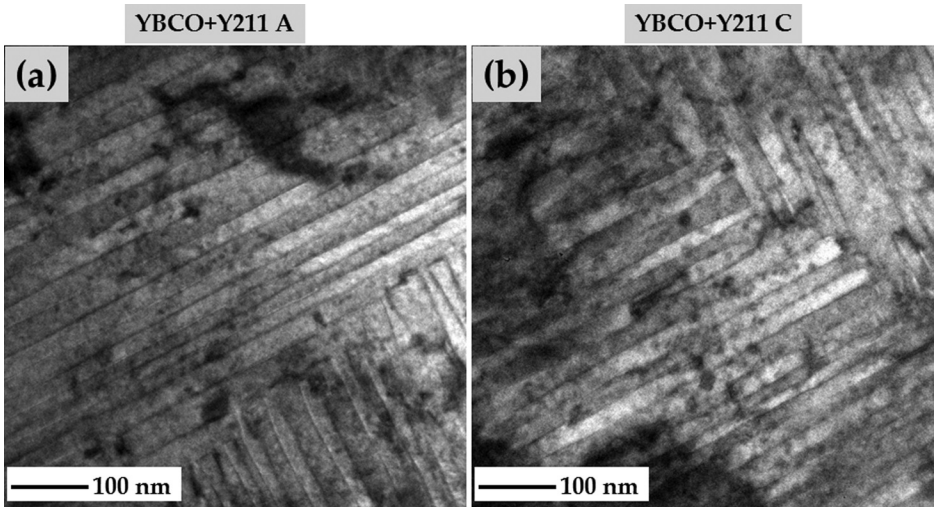


FIG. 6. The planar view of the microstructure exhibiting a high density of twin planes in (a) YBCO + Y211A and (b) YBCO + Y211C films. It can be observed that although the density of Y211 nanoinclusions is very different in these two films, the density of the twin planes is not much different.

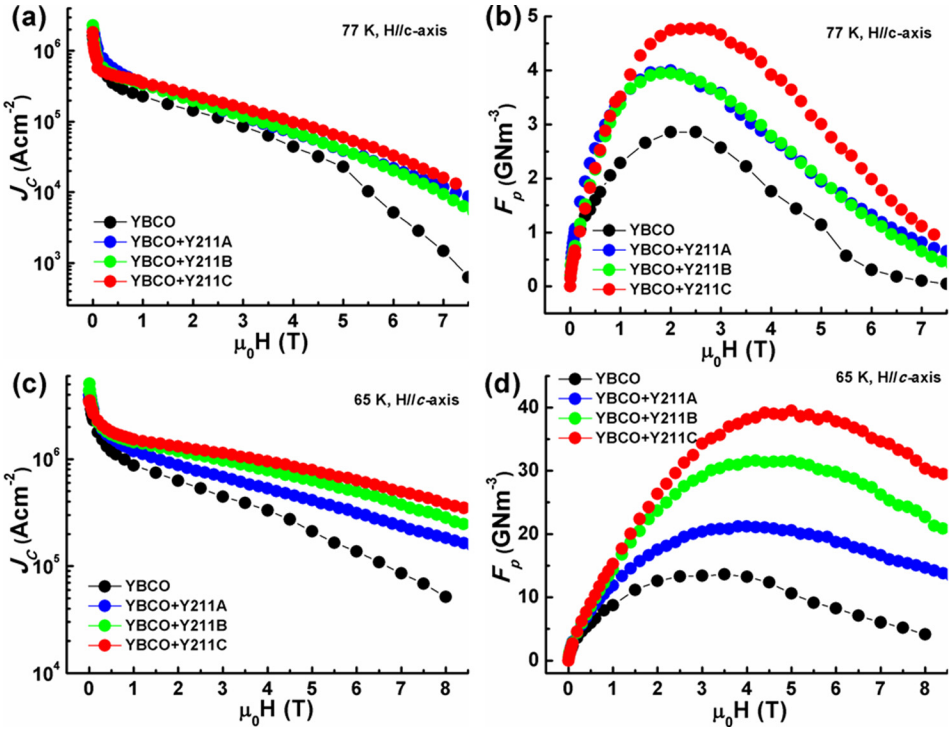


FIG. 7. Variation of critical current density ($J_C$) and pinning force density ($F_p$) with respect to applied magnetic field for YBCO and YBCO + Y211 nanocomposite films with varying concentrations of Y211 nanoparticles at 77 K (a), (b) and 65 K (c), (d). The in-field $J_C$ enhancement can be clearly observed for YBCO films with Y211 nanoinclusions.

has to be paid to move the fluxoid from the non-superconducting area, i.e., the fluxoid is pinned. The elementary pinning force, i.e., the force needed to depin a vortex line segment, is related to the pinning energy by the coherence length $\xi_{ab}$

$$f_p \approx \frac{U}{\xi_{ab}}. \tag{2}$$

If the flux line lattice is soft, i.e., the elastic energies are small compared to the pinning energies, each flux line will be individually pinned and the bulk pinning force per unit volume ($F_p$) is given by a direct summation over occupied pinning sites.

$$F_p = \Sigma f_p = N\frac{d_p}{a_0}f_p, \tag{3}$$

where $N$ is the number of pinning centers per unit volume, $d_p$ is the distance between two pinning centers, and $a_0$ is the distance between adjacent flux lines. This equation indicates that the bulk pinning force is proportional to the density of the pinning centers and $F_{pmax}$ values for nanocomposite films continue to increase with respect to Y211 nanoparticle density in nanocomposite films which means that the density of Y211 nanoparticles is below the optimum level. As the magnetic field is applied, Y211 nanoparticles provide stability to vortices against the Lorentz force and more APC translates to the prevention of the vortex motion against higher magnetic field.

In Fig. 8, the angular variation of $J_C$ for YBCO, YBCO + Y211A, YBCO + Y211B, and YBCO + Y211C films measured at (a) 77 K, 1 T and (b) 77 K, 3 T is presented. It can be observed that at 1 T, all the nanocomposite films exhibit isotropic enhancement in $J_C$ over a broad angular range except the YBCO + Y211C film which exhibits a continuous decrease and a dip near the *ab*-plane. Also, the *ab*-plane peak of YBCO + Y211A and YBCO + Y211B is similar to that of YBCO but for YBCO + Y211C, it is suppressed. At 77 K, 3 T, however, the YBCO + Y211C film exhibits maximum enhancement in $J_C$ over the entire investigated angular regime except along the *ab*-plane which indicates that high density of Y211 nanoparticles are effective for isotropic enhancement of $J_C$ at higher applied magnetic field. It is worth noting here that although the enhancement in $J_C$ is observed for most of the investigated angular regime, it is not observed along the *ab*-plane. It may be related to the density of the stacking faults (planar defects) which might not be very different in the nanocomposite films as observed in Fig. 4.

Figure 9 shows the angular dependent $J_C$ behavior of YBCO, YBCO + Y211A, YBCO + Y211B, and YBCO + Y211C films measured at (a) 65 K, 1 T (b) 65 K, 3 T, and (c) 65 K, 5 T. Isotropic enhancement in $J_C$ can be clearly observed for YBCO + Y211 nanocomposite films for a broad range of applied magnetic field orientation. However, as the orientation of the magnetic field approaches near the *ab*-plane, $J_C$ starts decreasing and reaches the minimum before again exhibiting a peak when applied magnetic field is along the *ab*-plane. In an earlier paper, Chudy *et al.*[11] reported the generation of APCs by neutron irradiation. Although the microstructure of the APC introduced samples is not presented in their report, it is presumed, on the basis of earlier literature, that the defects would be similar to the Y211 defects in the present paper. Also, despite the APC incorporation technique being different, the angular dependent $J_C$ behavior of the APC introduced samples exhibits striking similarities. It is to be noted here that although the authors have irradiated the HTS tapes by different neutron fluences,

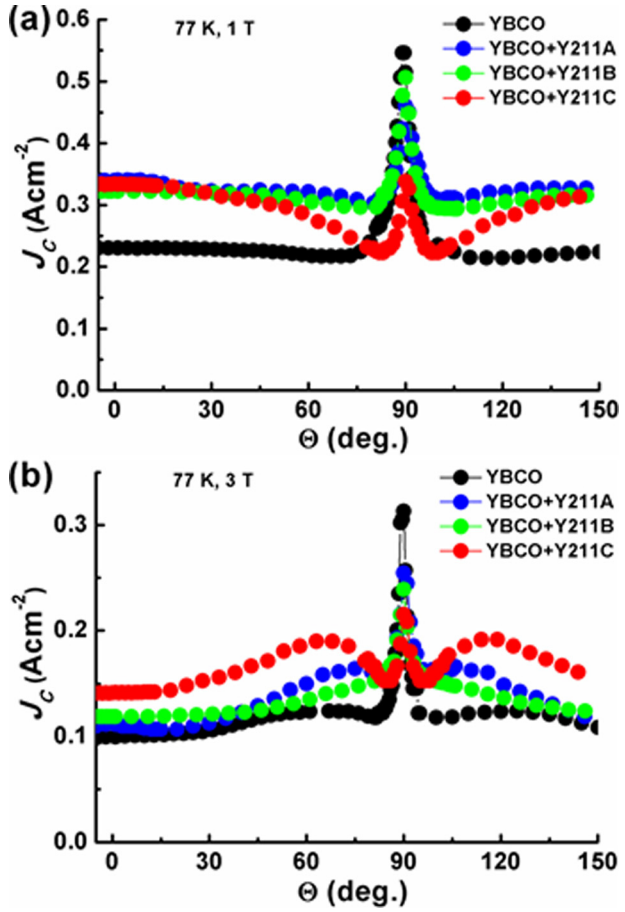


FIG. 8. Comparison of angular dependence of $J_C$ at (a) 77 K, 1 T and (b) 77 K, 3 T for YBCO and YBCO + Y211 nanocomposite films. The isotropic enhancement in the $J_C$ value along the broad angular regime can be observed for YBCO films with Y211 nanoparticles.

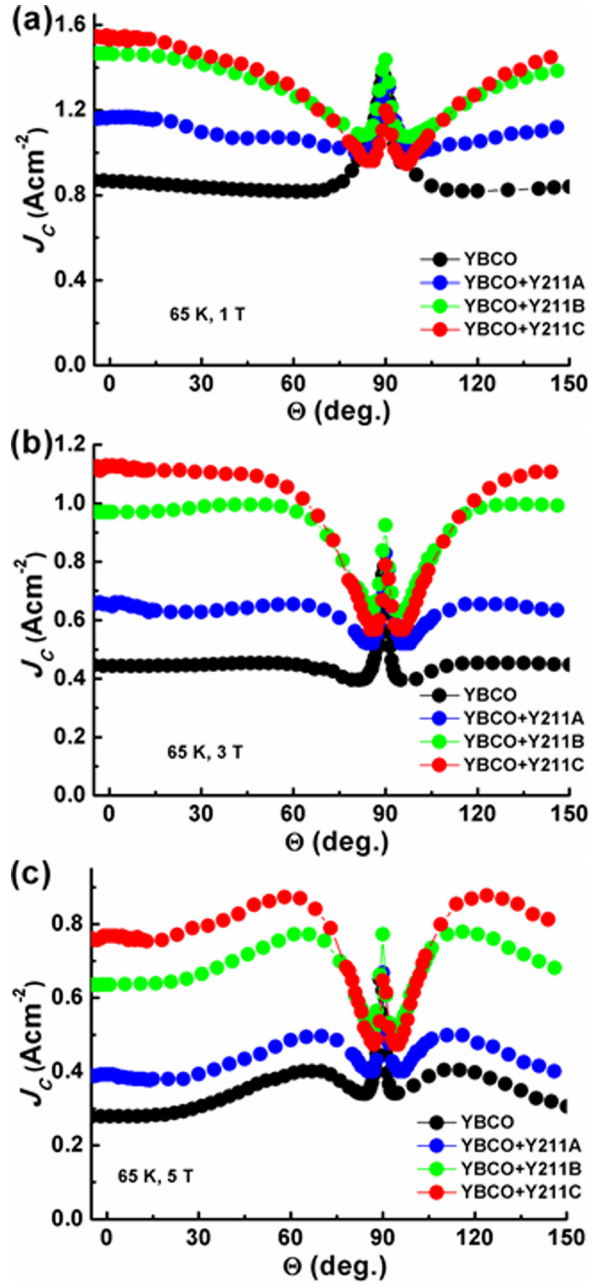


FIG. 9. Comparison of angular dependence of $J_C$ at (a) 65 K, 1 T, (b) 65 K, 3 T and (c) 65 K, 5 T for YBCO and YBCO + Y211 nanocomposite films. The isotropic enhancement in the $J_C$ value along the broad angular regime is more prominent and systematic at lower temperature.

the results of only one fluence ($2 \times 10^{21}$ m$^{-2}$) were presented in their report. Whereas, in the present paper, not only the systematic variation of Y211 nanoinclusion density is presented through microstructure examination but also its influence on the critical current properties is also studied which seem to vary systematically with respect to the Y211 content in the YBCO films. The enhancement in $J_C$ seems to be systematic with respect to the density of Y211 nanoinclusions: least being in YBCO + Y211A and maximum in YBCO + Y211C. In addition, it is noteworthy that the minimum $J_C$ has also increased considerably in YBCO + Y211 nanocomposite films.

The anisotropic scaling approach is very useful in the study of angular anisotropy of $J_C$ within collective pinning theory. It can be used to distinguish between random and correlated pinning in different angular regimes. This scaling approach was first proposed by Blatter *et al.*[59] and later successfully used by other researchers[33–35,42] to quantify the contribution of isotropic and anisotropic pinning in YBCO superconducting films. According to this approach, if pinning is caused by random defects, $J_C$ $(H,\theta)$ may be approximated to $J_C H\varepsilon(\theta)$ where

$$\varepsilon(\theta) = \sqrt{\left(\cos^2\theta + \gamma^{-2}\sin^2\theta\right)}, \tag{4}$$

and $\gamma$ (=5–7) is the electronic mass anisotropy parameter. In Fig. 10, the anisotropic scaling approach as applied to YBCO + Y211 films is presented. The black solid curve corresponds to the scaling curve obtained by using effective mass anisotropy ratio $\gamma_{\text{eff.}} = 2$ and 1.5 for YBCO + Y211A and YBCO + Y211C films, respectively, which indicates that intrinsic anisotropy is reduced as the Y211 nanoinclusions are increased in the Y123 matrix. The shape of the scaling curve matches well with the $J_C(\theta)$ within the angular interval of 25°–80° in the YBCO + Y211A film which means that $J_C$ in this angular interval is mainly caused by random pinning. However, in the case of the YBCO + Y211C film, the departure of $J_C(\theta)$ from the scaling curve towards the

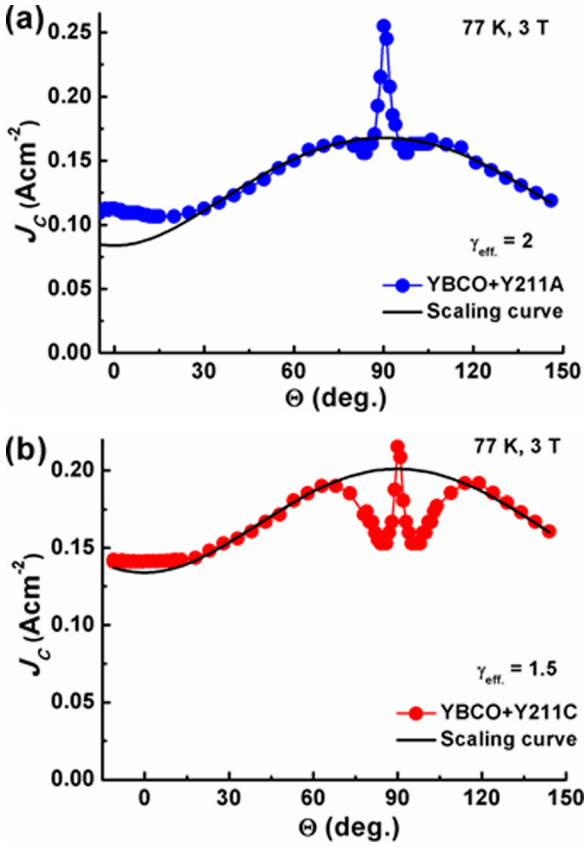


FIG. 10. Anisotropic scaling approach as applied to (a) YBCO + Y211A and (b) YBCO + Y211C nanocomposite films. The solid symbols represent the actual $J_C$, whereas the solid black line represents the scaling curve.

minima near the *ab*-plane may be attributed to a different depinning mechanism which cannot be described by the scaling approach. It is to be noted here that this anisotropic scaling approach can be applied to our films only in a high magnetic field case (3 T at 77 K). Looking at the $J_C(\theta)$ plots of the films at 65 K, it can be inferred that the anisotropic scaling approach cannot be applied as the shapes of the $J_C(\theta)$ curves are different at different applied magnetic fields, where local minima around $\theta = 0$ are absent. The efficiency of the random pinning centers due to Y211 nanoinclusions varies with the applied magnetic field and its orientation which is in contradiction with the collective pinning theory leads us to assume that pinning due to Y211 nanoinclusions and is not completely random.

In the case of interaction of the vortex with a non-superconducting defect, the pinning energy is proportional to the interaction volume which is mutually contributed by the pinning defect as well as the vortex itself. When applied field is oriented at an angle from the *c*-axis, the interaction volume between the vortex core and the defect is changed as the cross-section of the vortex core changes from circular to elliptical.[60] The cross-section of the vortex-core depends on the angle on inclination as per the following relationship:

$$\xi_{ab}(\theta) = \xi_{ab}\varepsilon(\theta). \tag{5}$$

At $\theta = 90°$, $\xi_{ab}(\theta) = \xi_c$. It has recently been suggested by Mishev *et al.*[60] that if the dimension of the spherical defect is smaller than the coherence length (such as point defects), the interaction volume between the vortex core and the defect will not change even if the applied magnetic field is oriented at any angle as the interaction volume will not change. However, if the size of the defect is larger than the coherence length (such as in the case of Y211 nanoinclusions), the interaction volume will change with respect to the inclination angle of the applied magnetic field which will result in the change in the pinning potential and the critical current density accordingly.

The appearance of the planar defects such as stacking faults is a commonly observed phenomenon in the Y123 films deposited by the PLD technique.[45,61] The formation of 124-type stacking faults results from an extra $CuO_2$ plane, forming in effect a monolayer of $YBa_2Cu_4O_8$ (Y124) instead of Y123 and these stacking faults assist in the propagation of planar defects. In a recent report, the stoichiometry of Y124 type structural defects has been investigated in detail by atomic resolution STEM (scanning transmission electron microscopy) analysis,[62] in which point defects associated with Cu and O vacancies were observed and it was proposed that the real cationic stoichiometry may be close to 1:2:3 instead of 1:2:4. The contribution of planar defects in the vortex pinning properties has recently been investigated by Yamasaki *et al.*[38] They proposed that these stacking faults themselves are weak planar pinning centers and the partial dislocations generated between the stacking fault/Y123 matrix interface act as linear pinning centers along the *ab*-plane. These linear pinning centers may act as the *ab*-plane correlated pinning centers when they are normally aligned to the current direction and as weak pinning centers otherwise. This assumption is similar to the one suggested by Matsumoto *et al.*[63] in Y123 films consisting of segmented BSO nanorods. The nanoscale strain due to partial dislocations associated with intergrowths generated between secondary phase nanoparticles and the Y123 matrix has been quantitatively evaluated[49,64] and has been proposed to be responsible for the suppression of Cooper-pair formation which results in enhanced vortex pinning efficiency of YBCO nanocomposite films.

In the case of linear/correlated pinning centers, the trapped length of the vortices decreases when the field is oriented at an angle with respect to the linear pinning centers.[65] The angle at which the trapped length of the vortices becomes zero is called accommodation angle. The expected vortex configuration due to the 3-D nanoparticles and 2-D planar defects for the case when applied magnetic field is inclined from the *ab*-plane is presented in Fig. 11. Nanoparticles pin the segments of the vortices connected by the unpinned portions. When the magnetic field is tilted from the *ab*-plane, the interaction volume between the nanoparticles and the vortex increases and subsequently, the pining energy due to the nanoparticles increases. Planar defects, on the other hand, behave as correlated pinning centers when the magnetic field is along the *ab*-plane, holding the vortices partially or completely depending on the width of the planar defect along the *c*-axis. When the magnetic field is tilted from the *ab*-plane, the length of the trapped portion of the vortices decreases and finally becomes negligibly small at the accommodation angle. The accommodation angle has been calculated by Paulius *et al.*[66]

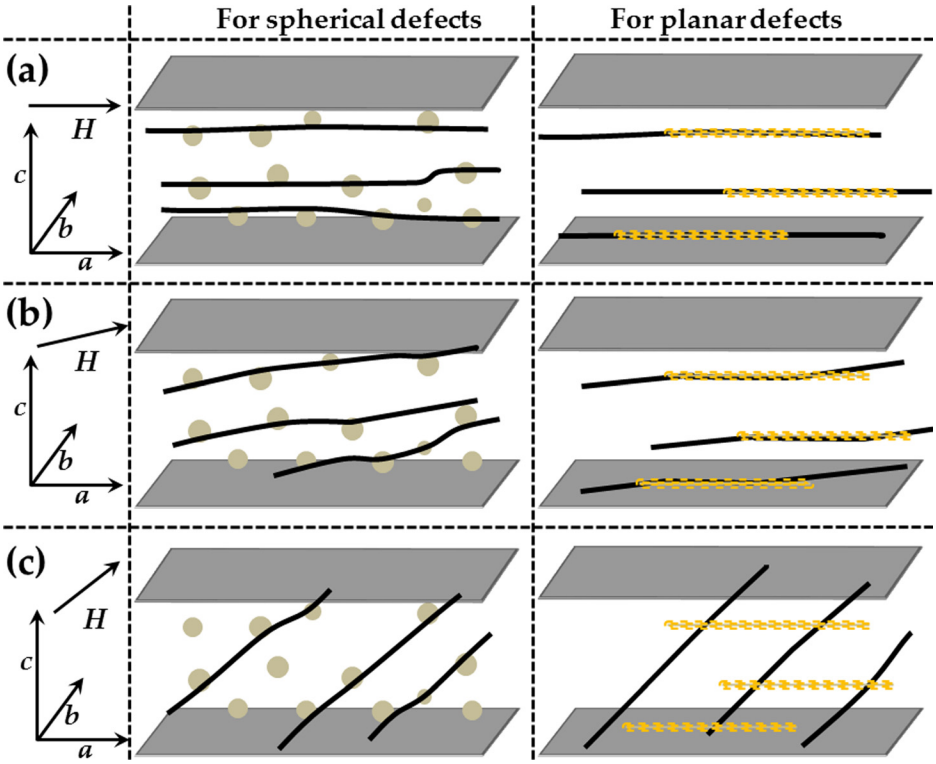


FIG. 11. Schematics of the possible vortex configuration due to 3-D nanoparticles and 2-D planar defects for different magnetic field orientations with respect to the *ab*-plane.

for YBCO single crystals subjected to heavy ion-irradiation resulting in the formation of columnar defects along the *c*-axis of the crystal. In the present case of YBCO + Y211 nanocomposite films, the pinning energy due to a planar defect can be estimated using Eq. (1). The length of the stacking fault resulting from the formation of the Y124 phase is much larger along the *ab*-plane than $\xi_{ab}$ at 65 K, but along the *c*-axis, it is only ∼0.2 nm (extension in the *c*-axis due to the additional $CuO_2$ plane) which is smaller than $\xi_c$ at 65 K.[49] The schematics of the interacting area of the vortex cross-section with a planar defect for the case when the thickness of the planar defect along the *c*-axis is larger or smaller than $\xi_c$ is shown in Fig. 12. The interacting cross-sectional area of the vortex with a planar defect, therefore, may be approximated as $\approx 2\xi_{ab}^{65\,\mathrm{K}} \times 0.2\,\mathrm{nm}$. The interaction volume, therefore, becomes $v_{int.} = 2\xi_{ab}^{65\,\mathrm{K}} \times 0.2\,\mathrm{nm} \times d$, where $d$ is the length of the planar defect along the *ab*-plane. Therefore, the pinning potential due to a planar defect is

$$U = \frac{B_C^2(65\,\mathrm{K})}{2\mu_0} \times \xi_{ab}^{65\mathrm{K}} \times 0.2\,\mathrm{nm} \times d,$$

using the standard values of the parameters and $d = 70\,\mathrm{nm}$, $U = 5.87 \times 10^{-20}\,\mathrm{J}$. Similarly, the pinning energy due to a Y211 nanoparticle of average diameter 5 nm can be calculated using Eq. (1) which comes out to be $2.53 \times 10^{-20}\,\mathrm{J}$, significantly smaller than due to a planar defect. However, for large inclinations of applied magnetic field from the *ab*-plane, the pinning energy due to planar pinning centers is negligibly smaller than that due to the 3-D nanoparticles. So, for most of the magnetic field orientations, the vortices are supposed to be arrested by the Y211 nanoparticles except for the regions near the *ab*-plane where planar defects dominate over the Y211 nanoparticles. The region of dominance of the planar defects is decided by the crossover angle where the vortices shift their locations between potentials due to spherical and planar defects. The pinning potential due to the linear pinning center is related to the accommodation angle as per the following relationship:

$$\tan\theta_{acc} = \sqrt{\frac{2u_p}{\epsilon_l}}, \tag{6}$$

where $\epsilon_l = \frac{\varphi_0^2}{4\pi\mu_0\lambda_{ab}^2}\ln\left(\frac{a_0}{\xi_{ab}}\right)$ is the line tension of the vortices, $u_p$ is the pinning energy per unit length of the defect, and $a_0 = \sqrt{\frac{\varphi_0}{B}}$ is the average separation among the vortices. For a particular case of the YBCO + Y211C sample at 65 K, 1 T, $\epsilon_l = 2.45 \times 10^{-11}\,\mathrm{J\,m^{-1}}$ and the accommodation angle is

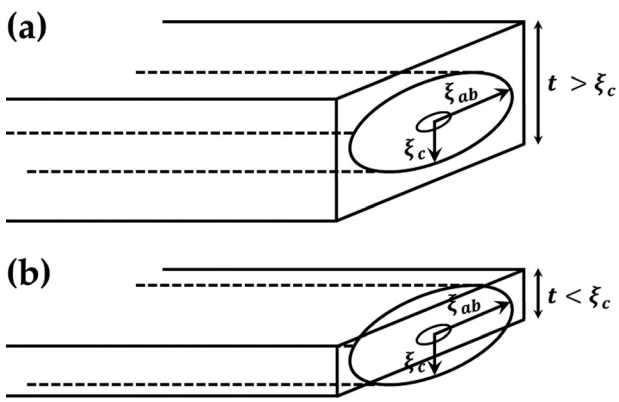


FIG. 12. Schematics of the interaction volume between a vortex and a planar defect for the case when the thickness of the planar defect along the *c*-axis is (a) larger than $\xi_c$ and (b) smaller than $\xi_c$.

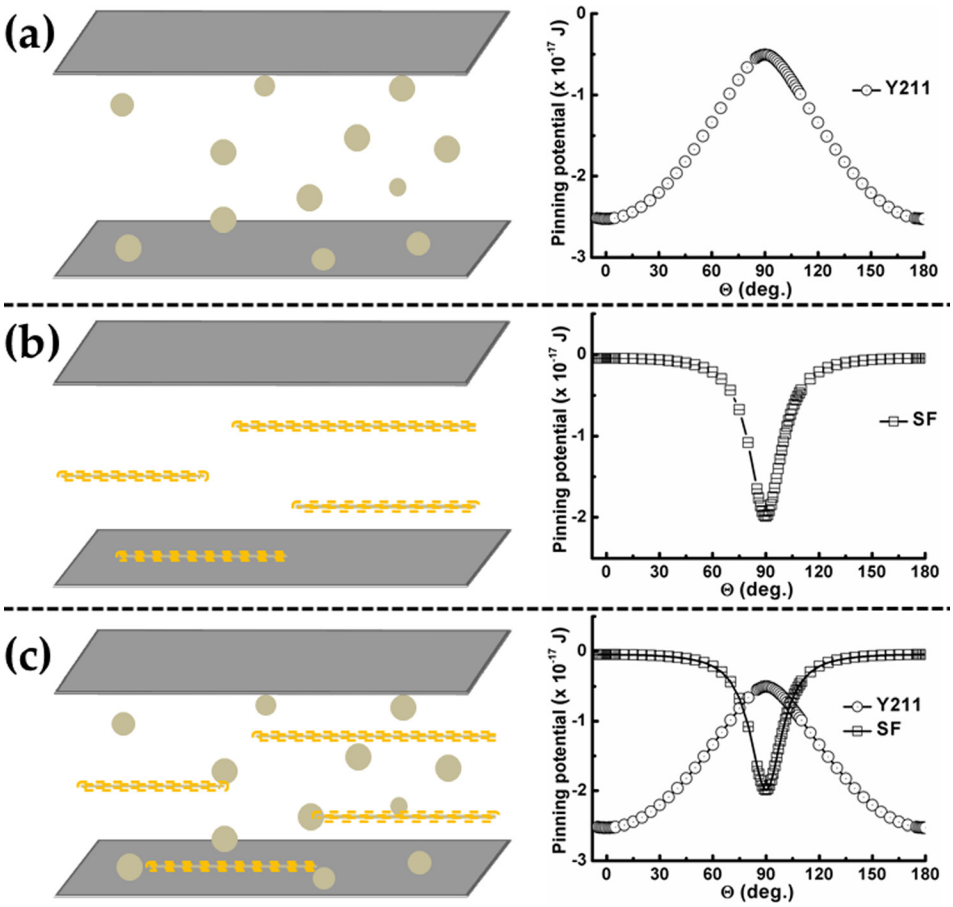


FIG. 13. Schematics of the pinning landscapes and the corresponding variation of the pinning potential as a function of magnetic field orientation. (a) Due to Y211 nanoparticles, (b) due to planar defects, and (c) due to the combination of both.

calculated from Eq. (6) which comes out to be 14.75°. Figure 13 represents the schematic diagram of the pinning landscape and the corresponding variation of the pinning potential with respect to the orientation of the applied magnetic field calculated using Eqs. (1) and (6) for the YBCO + Y211C film. In the hybrid APC case where both spherical and planar defects contribute to pinning, dominant pinning potential exhibits a crossover from pinning due to nanoparticles to pinning due to planar defects near the *ab*-plane. This crossover from one pinning potential to the other leads to the dip in the $J_C$-$B$-$\theta$ of the YBCO + Y211 nanocomposite films. Figure 14 represents the schematic diagram of localizing the vortices by spherical nanoparticles and planar defects. It can be visualized that spherical Y211 nanoparticles can effectively pin the vortices for most of the magnetic field orientations except near the *ab*-plane where the planar defect dominates in localizing the vortices. The intrinsic pinning associated with the periodic modulation of the order parameter arising from the layered structure of YBCO also contributes to *ab*-pinning. Thus, the movement of the vortices near the *ab*-plane from the defects associated with Y211 nanoparticles to the ones associated with the planar defects and weak pinning centers and vice-versa depending on the orientation of the magnetic field causes motion of the vortices near the *ab*-plane resulting in reduced $J_C$ and hence the dip in the $J_C - B - \theta$ plot near the *ab*-plane.

In the $J_C - B - \theta$ plot of the samples, the emergence of a broad $J_C$ peak is observed in the intermediate angular region at both 77 K and 65 K, at about 60°. It is to be noted that such peaks appear at relatively higher applied field (3 T at 77 K and 5 T at 65 K) and seem to dominate all other types of pinning at higher applied magnetic fields. Similar observations have previously been reported by Chudy *et al.*[11] and Ercolano *et al.*[67] It might be possible that the different pinning landscapes present in the films create an interacting network for a certain temperature/applied magnetic field combination which would act differently than the pinning

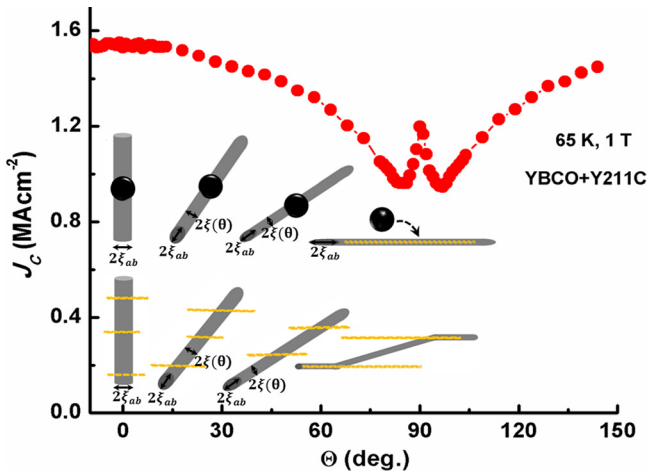


FIG. 14. Schematic illustration of contribution to vortex pinning by spherical and planar defects. With the inclination of the vortices from the *c*-axis, the interaction volume with the spherical defects reduces and the pinning energy is decreased resulting in an overall decrease in $J_C$. Planar defects such as stacking faults, on the other hand, are useful only for a limited angular regime and act as linear defects with a small accommodation angle.

landscapes would do it individually without any interaction. The vortex path model as suggested by Long[68] can be used to describe the occurrence of this additional peak in which the combination of Y211 nanostructures and planar pinning structures results in staircase vortices which experience strongest pinning at a particular angle determined by the particular distribution of defect lengths present in the superconducting matrix. This type of pinning is efficient at higher applied fields as it utilizes both kinds of pinning structures and hence strongly pins a greater vortex length. Such an interacting pinning network is expected to result in a complex depinning mechanism. However, it is not clearly understood and needs to be investigated in detail in future.

## IV. CONCLUSIONS

Y211 nanoparticles have been successfully incorporated into the YBCO film matrix in a systematic manner using surface modified target method and it has been shown that these Y211 nanoparticles are effective in improving the vortex pinning properties of YBCO thin films. $F_{pmax}$ values of the nanocomposite films exhibited a systematic increase with increasing the density of Y211 nanoinclusions and $\mu_0 H_{max}$ is shifted towards higher magnetic field which has been attributed to strong pinning of vortices by Y211 nanoparticles. An upper-shift in the irreversibility lines of the nanocomposite films was observed which has been attributed to cooperative vortex pinning contributions from the naturally occurring twin planes and Y211 nanoinclusions. Isotropic enhancement in the critical current density of the YBCO + Y211 nanocomposite films was observed both at 77 K and 65 K, supposedly due to the isotropic pinning provided by the Y211 nanoparticles. The dip in the $J_C - B - \theta$ plot near the *ab*-plane is discussed on the basis of competing nature of the pinning potentials due to isotropic pinning by Y211 nanoparticles and correlated pinning by planar defects along the *ab*-plane with a small accommodation angle.

## ACKNOWLEDGMENTS

This work is supported by the research startup grant provided by Kyushu Institute of Technology. A.K.J., P.M., and S.S. are thankful to Professor T. Suzuki, Graduate School of Advanced Sciences of Matter, Hiroshima University, Japan, for support on part of the transport measurements.

[1]K. Matsumoto and P. Mele, Supercond. Sci. Technol. **23**, 014001 (2010).
[2]S. R. Foltyn, L. Civale, J. L. MacManus Driscoll, Q. X. Jia, B. Maiorov, H. Wang, and M. Maley, Nat. Mater. **6**, 631 (2007).
[3]D. C. Larbalestier, A. Gurevich, D. M. Feldmann, and A. Polyanskii, Nature **414**, 368 (2001).
[4]R. Feenstra, D. K. Christen, C. E. Klabunde, and J. D. Budai, Phys. Rev. B **45**, 7555 (1992).
[5]B. Dam, J. M. Huijbregtse, F. C. Klaasen, R. C. F. Van der Geest, G. Doornbos, J. H. Rector, A. M. Testa, S. Freisem, J. C. Martinez, B. Stauble-Pumpin, and R. Griessen, Nature **399**, 439 (1999).
[6]H. Safar, S. Foltyn, H. Kung, M. P. Maley, J. O. Willis, P. Arendt, and X. D. Wu, Appl. Phys. Lett. **68**, 1853 (1996).
[7]C. Villard, G. Cohen, D. Cohen, E. Polturak, B. Thrane, and D. Chaterignier, Phys. Rev. Lett. **77**, 3913 (1996).
[8]A. Diaz, L. Mechin, P. Berghuis, and J. E. Evetts, Phys. Rev. Lett. **80**, 3855 (1998).
[9]T. Sueyoshi, T. Sogo, T. Nishimura, T. Fujiyoshi, F. Mitsugi, T. Ikegami, S. Awaji, K. Watanabe, A. Ichinose, and N. Ishikawa, Supercond. Sci. Technol. **29**, 065023 (2016).
[10]Y. Jia, M. LeRoux, D. J. Miller, J. G. Wen, W. K. Kwok, U. Welp, M. W. Rupich, X. Li, S. Sathyamurthy, S. Fleshler, A. P. Malozemoff, A. Kayani, O. Ayala-Valenzuela, and L. Civale, Appl. Phys. Lett. **103**, 122601 (2013).
[11]M. Chudy, R. Fuger, M. Eisterer, and H. W. Weber, IEEE Trans. Appl. Supercond. **21**, 3162 (2011).
[12]M. Chudy, M. Eisterer, and H. W. Weber, Physica C **470**, 1300 (2010).
[13]C. Cai, B. Holzapfel, J. Hanishch, L. Fernandez, and L. Schultz, Phys. Rev. B **69**, 104531 (2004).
[14]S. H. Wee, A. Goyal, P. M. Martin, and L. Heatherly, Supercond. Sci. Technol. **19**, 865 (2006).
[15]T. Haugan, P. N. Barnes, R. Wheeler, F. Meisenkothen, and M. Sumption, Nature **430**, 867 (2004).
[16]C. V. Varanasi, P. N. Barnes, J. Burke, J. Carpenter, and T. J. Haugan, Appl. Phys. Lett. **87**, 262510 (2005).
[17]P. Mele, R. Guzman, J. Gazquez, T. Puig, X. Obradors, S. Saini, Y. Yoshida, M. Mukaida, A. Ichinose, K. Matsumoto, and M. I. Adam, Supercond. Sci. Technol. **28**, 024002 (2015).
[18]A. A. Gapud, D. Kumar, S. K. Viswanathan, C. Cantoni, M. Varela, J. Abiade, S. J. Pennycook, and D. K. Christen, Supercond. Sci. Technol. **18**, 1502 (2005).
[19]P. Mele, K. Matsumoto, A. Ichinose, M. Mukaida, Y. Yoshida, S. Horii, and R. Kita, Supercond. Sci. Technol. **21**, 125017 (2008).
[20]C. V. Varanasi, J. Burke, H. Wang, J. H. Lee, and P. N. Barnes, Appl. Phys. Lett. **93**, 092501 (2008).
[21]C. V. Varanasi, J. Burke, L. Brunke, H. Wang, M. Sumption, and P. N. Barnes, J. Appl. Phys. **102**, 063909 (2007).
[22]H. Yang, H. Wang, B. Maiorov, J. Lee, D. Talbayev, M. J. Hinton, D. M. Feldmann, J. L. MacManus-Driscoll, A. J. Taylor, L. Civale, T. R. Lemberger, and Q. X. Jia, J. Appl. Phys. **106**, 093914 (2009).
[23]J. L. MacManus Driscoll, S. R. Foltyn, Q. X. Jia, H. Wang, A. Serquis, L. Civale, B. Maiorov, M. E. Hawley, M. P. Maley, and D. E. Peterson, Nat. Mater. **3**, 439 (2004).
[24]A. Goyal, S. Kang, K. J. Leonard, P. M. Martin, A. A. Gapud, M. Varela, M. Paranthaman, A. O. Ijaduola, E. D. Specht, J. R. Thompson, D. K. Christen, S. J. Pennycook, and F. A. List, Supercond. Sci. Technol. **18**, 1533 (2005).
[25]J. Hanisch, C. Cai, R. Huhne, L. Schultz, and B. Holzapfel, Appl. Phys. Lett. **86**, 122508 (2005).
[26]S. H. Wee, A. Goyal, E. D. Specht, C. Cantoni, Y. L. Zuev, V. Selvamanickam, and S. Cook, Phys. Rev. B **81**, 140503 (2010).
[27]D. M. Feldmann, T. G. Holesinger, B. Maiorov, S. R. Foltyn, J. Y. Coulter, and I. Apodaca, Supercond. Sci. Technol. **23**, 095004 (2010).
[28]S. H. Wee, A. Goyal, Y. L. Zuev, C. Cantoni, V. Selvamanickam, and E. D. Specht, Appl. Phys. Express **3**, 023101 (2010).
[29]A. K. Jha, N. Khare, and R. Pinto, J. Appl. Phys. **110**, 113920 (2011).
[30]T. Aytug, M. Paranthaman, K. J. Leonard, K. Kim, A. O. Ijaduola, Y. Zhang, E. Tuncer, J. R. Thompson, and D. K. Christen, J. Appl. Phys. **104**, 043906 (2008).
[31]T. Aytug, M. Paranthaman, A. A. Gapud, S. Kang, H. M. Christen, K. J. Leonard, P. M. Martin, J. R. Thompson, D. K. Christen, R. Meng, I. Rusakova, C. W. Chu, and T. H. Johansen, J. Appl. Phys. **98**, 114309 (2005).
[32]M. Coll, S. Ye, V. Rouco, A. Palau, R. Guzman, J. Gazquez, J. Arbiol, H. Suo, T. Puig, and X. Obradors, Supercond. Sci. Technol. **26**, 015001 (2013).
[33]X. Obradors, T. Puig, S. Ricart, M. Coll, J. Gazquez, A. Palau, and X. Granados, Supercond. Sci. Technol. **25**, 123001 (2012).
[34]T. Puig, J. Gutierrez, A. Pomar, A. Llordes, J. Gazquez, S. Ricart, F. Sandiumenge, and X. Obradors, Supercond. Sci. Technol. **21**, 034008 (2008).
[35]J. Gutierrez, A. Llordes, J. Gazquez, M. Gibert, N. Roma, S. Ricart, A. Pomar, F. Sandiumenge, N. Mestres, T. Puig, and X. Obradors, Nat. Mater. **6**, 367 (2007).
[36]S. Engel, T. Thersleff, R. Hühne, L. Schultz, and B. Holzapfel, Appl. Phys. Lett. **90**, 102505 (2007).
[37]H. Yamasaki, K. Ohki, H. Yamada, Y. Nakagawa, and Y. Mawatari, Supercond. Sci. Technol. **21**, 125011 (2008).
[38]H. Yamasaki, K. Ohki, I. Yamaguchi, M. Sohma, W. Kondo, H. Matsui, T. Manabe, and T. Kumagai, Supercond. Sci. Technol. **23**, 105004 (2010).
[39]H. Yamasaki, Supercond. Sci. Technol. **29**, 065005 (2016).

[40]M. Tachiki and S. Takahashi, Solid State Commun. **70**, 291 (1989).
[41]M. Tachiki and S. Takahashi, Solid State Commun. **72**, 1083 (1989).
[42]L. Civale, B. Maiorov, A. Serquis, J. O. Willis, J. Y. Coulter, H. Wang, Q. X. Jia, P. N. Arendt, J. L. MacManus Driscoll, M. P. Maley, and S. R. Foltyn, Appl. Phys. Lett. **84**, 2121 (2004).
[43]A. K. Jha, K. Matsumoto, T. Horide, S. Saini, P. Mele, A. Ichinose, Y. Yoshida, and S. Awaji, Supercond. Sci. Technol. **28**, 114004 (2015).
[44]S. K. Viswanathan, A. A. Gapud, M. Varela, J. T. Abiade, D. K. Christen, S. J. Pennycook, and D. Kumar, Thin Solid Films **515**, 6452 (2007).
[45]A. K. Jha, K. Matsumoto, T. Horide, S. Saini, P. Mele, Y. Yoshida, and S. Awaji, Supercond. Sci. Technol. **27**, 025009 (2014).
[46]A. Catana, R. F. Broom, J. G. Bednorz, J. Manhart, and D. G. Schlom, Appl. Phys. Lett. **60**, 1016 (1992).
[47]O. Eibl and B. Roas, J. Mater. Res. **5**, 2620 (1990).
[48]M. Miura, M. Yoshizumi, T. Izumi, and Y. Shiohara, Supercond. Sci. Technol. **23**, 014013 (2010).
[49]A. Llordes, A. Palau, J. Gazquez, M. Coll, R. Vlad, A. Pomar, J. Arbiol, R. Guzman, S. Ye, V. Rouco, F. Sandiumenge, S. Ricart, T. Puig, M. Varela, D. Chateigner, J. Vanacken, J. Gutierrez, V. Moshchalkov, G. Deutscher, C. Magen, and X. Obradors, Nat. Mater. **11**, 329 (2012).
[50]H. Y. Zhai and W. K. Chu, Appl. Phys. Lett. **76**, 3469 (2000).
[51]X. Obradors and T. Puig, Supercond. Sci. Technol. **27**, 044003 (2014).
[52]L. Krusin-Elbaum, L. Civale, J. R. Thompson, and C. Field, Phys. Rev. B **53**, 11744 (1996).
[53]S. Horii, M. Haruta, A. Ichinose, and T. Doi, J. Appl. Phys. **118**, 133907 (2015).
[54]T. Ozaki, Y. Yoshida, Y. Ichino, Y. Takai, A. Ichinose, K. Matsumoto, S. Horii, M. Mukaida, and Y. Takano, J. Appl. Phys. **108**, 093905 (2010).
[55]M. Miura, B. Maiorov, F. F. Balakirev, T. Kato, M. Sato, Y. Takagi, T. Izumi, and L. Civale, Sci. Rep. **6**, 20436 (2016).
[56]M. Miura, S. A. Baily, B. Maiorov, L. Civale, J. O. Willis, K. Marken, T. Izumi, K. Tanabe, and Y. Shiohara, Appl. Phys. Lett. **96**, 072506 (2010).
[57]R. Guzman, J. Gazquez, V. Rouco, A. Palau, C. Magen, M. Varela, J. Arbiol, X. Obradors, and T. Puig, Appl. Phys. Lett. **102**, 081906 (2013).
[58]V. Rouco, A. Palau, R. Guzman, J. Gazquez, M. Coll, X. Obradors, and T. Puig, Supercond. Sci. Technol. **27**, 125009 (2014).
[59]G. Blatter, V. B. Geshkenbein, and A. I. Larkin, Phys. Rev. Lett. **68**, 875 (1992).
[60]V. Mishev, M. Zehetmayer, D. X. Fischer, M. Nakajima, H. Eisaki, and M. Eisterer, Supercond. Sci. Technol. **28**, 102001 (2015).
[61]S. H. Wee, Y. L. Zuev, C. Cantoni, and A. Goyal, Sci. Rep. **3**, 2310 (2013).
[62]J. Gazquez, R. Guzman, R. Mishra, E. Bartolome, J. Salafranca, C. Magen, M. Varela, M. Coll, A. Palau, S. M. Valvidares, P. Gargiani, E. Pellegrin, J. Herrero-Martin, S. J. Pennycook, S. T. Pantelides, T. Puig, and X. Obradors, Adv. Sci. **3**, 1500295 (2016).
[63]K. Matsumoto, I. Tanaka, T. Horide, P. Mele, Y. Yoshida, and S. Awaji, J. Appl. Phys. **116**, 163903 (2014).
[64]R. Guzman, J. Gazquez, B. Mundet, M. Coll, X. Obradors, and T. Puig, Phys. Rev. Mater. **1**, 024801 (2017).
[65]G. Blatter, M. V. Feigel'man, V. B. Geshkenbein, A. I. Larkin, and V. M. Vinokur, Rev. Mod. Phys. **66**, 1125 (1994).
[66]L. M. Paulius, J. A. Fendrich, W. K. Kwok, A. E. Koshelev, V. M. Vinokur, G. W. Crabtree, and B. G. Glagola, Phys. Rev. B. **56**, 913 (1997).
[67]G. Ercolano, M. Bianchetti, S. C. Wimbush, S. A. Harrington, H. Wang, J. H. Lee, and J. L. MacManus-Driscoll, Supercond. Sci. Technol. **24**, 095012 (2011).
[68]N. J. Long, Supercond. Sci. Technol. **21**, 025007 (2008).